New set of sensitivity runs for "Air-snowpack exchange of bromine, ozone and mercury in the springtime Arctic simulated by the 1-D model PHANTAS – Part 2: Mercury and its speciation" in revision for Atmospheric Chemistry and Physics

K. Toyota[1,2], A. P. Dastoor[3], and A. Ryzhkov[3]

[1]Department of Earth and Space Science and Engineering, York University, Toronto, Ontario, Canada
[2]Air Quality Modelling and Integration Section, Environment Canada, Toronto, Ontario, Canada
[3]Air Quality Modelling and Integration Section, Environment Canada, Dorval, Quebec, Canada

Correspondence to: K. Toyota (kenjiro.toyota@ec.gc.ca)

1 Scientific background

It is believed that mercury oxidation during the AMDEs results mostly from a series of gas-phase reactions initiated via Br-attack on Hg(0):

$$Hg + Br\ (+M) \rightarrow HgBr. \qquad (R1)$$

Subsequently, a part of HgBr undergoes a thermal decomposition back to Hg and Br:

$$HgBr\ (+\ M) \rightarrow Hg + Br, \qquad (R2)$$

which is competed by further reactions of HgBr to form thermally stable products such as $HgBr_2$:

$$HgBr + Br\ (+\ M) \rightarrow HgBr_2. \qquad (R3a)$$

According to a quantum chemistry study by Balabanov et al. (2005), there are two other product channels in the reaction between HgBr + Br, namely, Br-exchange (R3b) and Br-abstraction (R3c):

$$HgBr + Br \rightarrow BrHg + Br \qquad (R3b)$$
$$Hg + Br_2. \qquad (R3c)$$

In this section, we summarize what is known about rate constant for each of these reactions, on the basis of our literature survey.

1.1 HgBr + Br (+ M) → HgBr (R1)

Donohue et al. (2006) conducted a laboratory kinetic study to determine the rate coefficient for the reaction (R1) using N_2 as buffer gas for the temperature range of 243-293 K and the pressure range of 200-600 Torr (760 Torr = 1 atm) and using He as buffer gas for the pressure range of 200-600 Torr at room temperature. Their experimental results in the N_2 buffer gas were fitted to temperature-dependent, third-order rate coefficient:

$$k_{1,\ \mathrm{Donohue}} = (1.46\pm0.34)\times10^{-32}\times(T/298)^{(-1.86\pm1.49)}\ \ [\mathrm{cm^6\ molecule^{-2}\ s^{-1}}].$$

By using the Rice-Ramsberg-Kassel-Marcus (RRKM) theory with ab initio calculations of bond energies at the B3LYP level of theory, Goodsite et al. (2012) derived the third-order rate constant for the same reaction at T = 200-300 K:

$$k_{1,\ \mathrm{Goodsite}} = 1.5\times10^{-32}\times(T/298)^{-1.76}\ \ [\mathrm{cm^6\ molecule^{-2}\ s^{-1}}]$$

which gives values in excellent agreement with experimentally derived ones by Donohue et al. (2006). Shepler et al. (2007) used a higher level of theory, namely, CCSD(T) (coupled cluster theory with single and double excitations and a perturbative treatment of triple excitations) for ab initio calculations to construct the potential energy surface of the reaction dynamics for Hg + Br + Ar → HgBr + Ar, which is then used to derive the temperature-dependent rate constant by the quasi-classical trajectories (QCT) method:

$$k_{1,\ \mathrm{Shepler}} = 4.07\times10^{-32}\ \exp[112\ (1/T - 1/298)]\ \ [\mathrm{cm}^6\ \mathrm{molecule}^{-2}\ \mathrm{s}^{-1}].$$

Between 200-320 K this rate constant by Shepler et al. (2007) gives values a factor of 2-3 greater than those derived by Donohue et al. (2006) and Goodsite et al. (2012). Even higher rate constants were derived by earlier theoretical calculations such as Khalizov et al. (2003) (Fig. 1; see also Shepler et al., 2007).

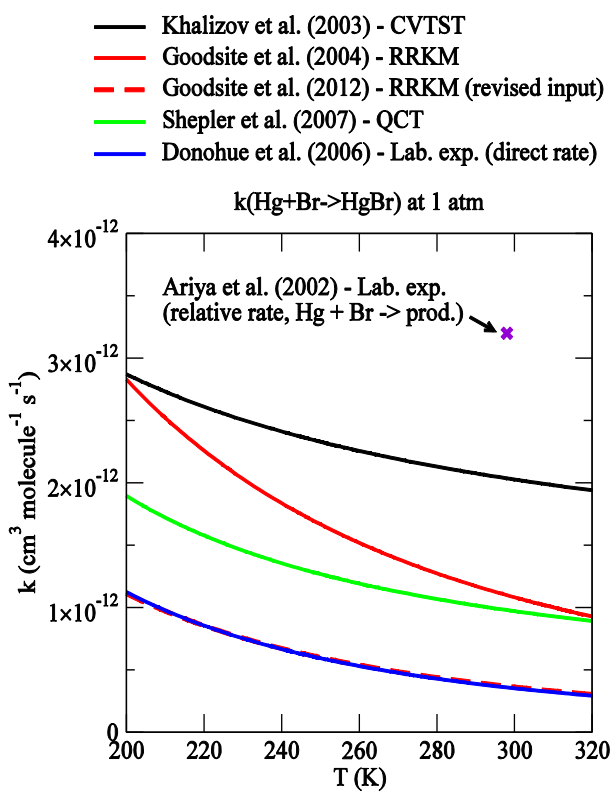

Figure 1: Comparison between rate constants for the reaction (R1) in the second-order expression at 1 atm as calculated theoretically (Khalizov et al., 2003; Goodsite et al., 2004, 2012; Shepler et al., 2007) or derived experimentally (Ariya et al., 2002; Donohue et al., 2006). Note, however, that the Ariya et al. data would likely represent the rate constant for net reaction including R2 and R3a-c subsequent to R1 as well as heterogeneous reactions mediated on the surface of reactor wall.

1.2 HgBr (+ M) → Hg + Br (R2)

There has been no experimental determination but theoretical calculations of the rate constant for this reaction. By using the same methodology to derive the rate constant for R1 (see Section 1.1), Goodsite et al. (2012) obtained the following first-order expression for R2 with M = N_2 at 1 atm and between 200-300 K:

$$k_{2,\ \mathrm{Goodsite}} = 4.0\times10^{9}\ \exp(-7292/T)\ \ [\mathrm{s}^{-1}].$$

If we assume the low-pressure limit behavior for R2, we may re-write this rate constant in the second-order expression:

$$k_{2,\ \mathrm{Goodsite}}' = 1.62\times10^{-10}\times(T/298)\times\exp(-7292/T)\ \ [\mathrm{cm}^3\ \mathrm{molecule}^{-1}\ \mathrm{s}^{-1}].$$

On the order hand, by using CCSD(T) and QCT methods, Shepler et al. (2007) derived the following second-order rate constant for R2 with M = Ar:

$$k_{2,\ \mathrm{Shepler}} = 1.95\times10^{-20}\ \exp[112\ (1/T - 1/298)]\ \ [\mathrm{cm^6\ molecule^{-2}\ s^{-1}}].$$

which gives values a factor of 4-5 greater than those derived by Goodsite et al. (2012) between T = 200-320 K (see Fig. 2).

On the other hand, Dibble et al. (2012, 2013) calculated bond energy for HgBr by the CCSD(T) level of theory and derived a thermodynamic equilibrium constant for the reactions R1 and R2, viz. Hg + Br + M = HgBr + M, as $K_{eq} = (9.14\pm0.06)\times10^{-24}\ \exp[(7801\pm201)/T]\ \mathrm{cm^3\ molecule^{-1}}$. By taking the rate constant for R1 from Donohue et al. (2006), these authors calculate the rate constant for R2:

$$k_{2,\ \mathrm{Dibble}} = (1.60\pm0.37)\times10^{-9}\times(T/298)^{(-1.86\pm1.49)} \times \exp[(-7801\pm201)/T]\ \ [\mathrm{cm^3\ molecule^{-1}\ s^{-1}}]$$

which gives values between those calculated by Shepler et al. (2007) and Goodsite et al. (2012).

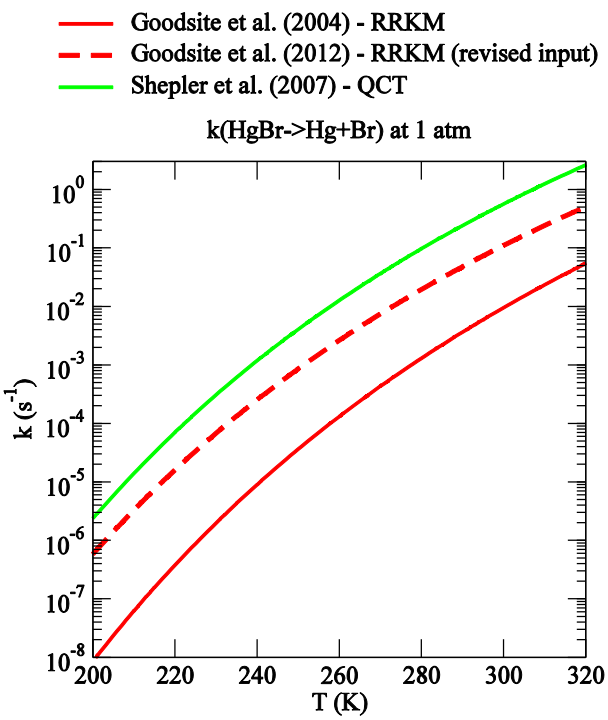

Figure 2: Comparison between rate constants for the reaction (R2) in the first-order expression at 1 atm as calculated theoretically (Goodsite et al., 2004, 2012; Shepler et al., 2007).

1.3 HgBr + Br (+ M) → $HgBr_2$ (R3a), BrHg + Br (R3b) or Hg + Br_2 (R3c)

Again, there is no experimental determination of the rate constant(s) for R3. By using the RRKM theory with ab initio calculations of bond energies at the B3LYP level of theory, Goodsite et al. (2004) derived the rate constant for R3a with M = N_2 at 1 atm and between 180-400 K:

$$k_{3a,\ \mathrm{Goodsite}} = 2.5\times10^{-10}\times(T/298)^{-0.57}\ \ [\mathrm{cm^3\ molecule^{-1}\ s^{-1}}]$$

where the reaction is close to the high-pressure limit at 1 atm and thus rationalizes the second-order expression. Goodsite et al. (2012), however, later revised input data for the bond energy of HgBr for re-calculation of the rate constants for the reactions (R1) and (R2). Unfortunately, the rate constant for R3a was not recalculated in Goodsite et al. (2012).

Balabanov et al. (2005) employed the CCSD(T) level of theory with the QCT method, viz. the same methodology as employed by Shepler et al. (2007) for the rate constant calculations for R1 and R2, to calculate the rate constants for R3a, R3b and R3c at 298 K:

$k_{3a,\ Balabanov\text{-}QCT} = (2.98\pm0.14)\times10^{-11}$ [cm^3 $molecule^{-1}$ s^{-1}]
$k_{3b,\ Balabanov\text{-}QCT} = (3.97\pm0.35)\times10^{-11}$ [cm^3 $molecule^{-1}$ s^{-1}]
$k_{3c,\ Balabanov\text{-}QCT} = (3.89\pm0.17)\times10^{-11}$ [cm^3 $molecule^{-1}$ s^{-1}].

The k_{3a} value calculated by Balabanov et al. is a factor of 8 lower than that calculated at 298 K by Goodsite et al. (2004). Balabanov et al. attributed this discrepancy primarily to the lower level of theory (i.e., B3LYP method) employed by Goodsite et al. for estimating input parameters of the RRKM calculation. Also, QCT-derived rate constants for R3a-c by Balabanov et al. represent the reactions in the low-pressure limit and hence may have underestimated the collision-induced deactivation of exited states of $HgBr_2$ along the trajectories of reaction dynamics. Balabanov et al. speculated that, by taking this effect in account, the value of k_{3a} could be raised while in compensation reducing the value of k_{3b} for the Br-exchange channel (R3b). It should be noted that even the sum of $k_{3a,\ Balabanov\text{-}QCT}$ and $k_{3b,\ Balabanov\text{-}QCT}$ is 3.6 times lower than $k_{3a,\ Goodsite}$ at 298 K.

Goodsite et al. (2004) also calculated the bond energies of BrHg-I and BrHg-OH and found them to be only slightly lower than that of BrHg-Br, indicating the involvement of I-atom and OH-radical in the formation of divalent mercury in the background tropospheric air. On the basis of bond energies calculated by the CCSD(T) level of theory, Dibble et al. (2012) indicated that reactions of HgBr with HO_2, NO_2, BrO and ClO would also be viable in the atmosphere.

2 New sensitivity runs on uncertainty in the gas-phase mechanism of Hg oxidation

2.1 Experiment setup

All the physical and chemical conditions employed here are the same as reported in Toyota et al. (2013a, 2013b) unless otherwise stated below for conducting the present sensitivity study. Also changed in the present model runs from Toyota et al. is the vertical diffusivity of condensed-phase species across the LLL network of snowpack; it is now scaled down by a factor of 10 from the value approximated by self-diffusivity of H_2O molecules in bulk super-cooled water. According to a molecular dynamics simulation by Carignano et al. (2007) of Na^+ and Cl^- ions in the surface disordered layer of ice, ion diffusivity is reduced by an order of magnitude in a thin liquid-like layer as compared to that in a thick liquid layer at the same temperature (260 K).

In each of test scenarios with different combination of rate constants for the reactions R1 to R3 (Table 1), model runs are performed for meteorological conditions at the temperature of 253 K, the reference-height wind speeds of 2 m/s, 4.5 m/s, 8.5 m/s or 12 m/s under the clear sky on March 30 at the latitude of 70 °N. Excellent agreement between the laboratory experiment by Donohue et al. (2006) and the theoretical calculation by Goodsite et al. (2012) gives some confidence in adopting the rate constant(s) for R1 from these studies (Scenarios 1-3). Nevertheless, the fact that Shepler et al. (2007) employed a higher level of theory than Goodsite et al. (2012) rationalizes to test the higher rate constant for R1 adopted from Shepler et al. (Scenario 4). In Scenario 1, the thermal decomposition of HgBr (R2) and the stabilization of HgBr via Br-addition (R3a) are assumed to follow the rate constants determined via B3LYP/RRKM calculations in Goodsite et al. (2004, 2012). In Scenarios 2 to 4, we adopt the rate constants for these reactions from Balabanov et al. (2005) and Shepler et al. (2007) both of which employed CCSD(T)/QCT calculations. All the scenarios adopt the rate constant for the Br-abstraction

channel of the reaction HgBr + Br (R3c) from Balabanov et al. (2005). In addition to changing the rate constants for R1-3, we switch on and off for the reaction HgBr + BrO → Hg(OBr)Br (for which the same rate constant as that for R3a is assumed) and change the empirically-adjusted rates for in-snow photo-reduction of Hg(II) between "slow" and "fast" photo-reduction scenarios following Johnson et al. (2008) and Kirk et al. (2006), respectively (Table 2, see also Toyota et al., 2013b).

Table 1: List of rate constants for the gas-phase reactions of mercury varied between sensitivity runs.

Reaction	Rate constant	Unit	Rreference
	Scenario 1		
Hg + Br + M → HgBr + M	1.44×10^{-32} $(T/300)^{-1.86}$ [M]	cm^3 $molec.^{-1}$ sec^{-1}	Donohue et al. (2006)
HgBr + M → Hg + Br + M	4.0×10^{9} exp(-7292/T)	sec^{-1}	Goodsite et al. (2012)
HgBr + Br → $HgBr_2$	2.5×10^{-10} $(T/300)^{-0.57}$	cm^3 $molec.^{-1}$ sec^{-1}	Goodsite et al. (2004)
HgBr + BrO → Hg(OBr)Br	2.5×10^{-10} $(T/300)^{-0.57}$	cm^3 $molec.^{-1}$ sec^{-1}	(= $k_{HgBr + Br}$)
	Scenario 2		
Hg + Br + M → HgBr + M	1.44×10^{-32} $(T/300)^{-1.86}$ [M]	cm^3 $molec.^{-1}$ sec^{-1}	Donohue et al. (2006)
HgBr + M → Hg + Br + M	2.94×10^{-9} exp(-7670/T)	cm^3 $molec.^{-1}$ sec^{-1}	Shepler et al. (2007)
HgBr + Br → $HgBr_2$	2.98×10^{-11}	cm^3 $molec.^{-1}$ sec^{-1}	Balabanov et al. (2005)
HgBr + BrO → Hg(OBr)Br	2.98×10^{-11}	cm^3 $molec.^{-1}$ sec^{-1}	(= $k_{HgBr + Br}$)
	Scenario 3		
Hg + Br + M → HgBr + M	1.44×10^{-32} $(T/300)^{-1.86}$ [M]	cm^3 $molec.^{-1}$ sec^{-1}	Donohue et al. (2006)
HgBr + M → Hg + Br + M	2.94×10^{-9} exp(-7670/T)	cm^3 $molec.^{-1}$ sec^{-1}	Shepler et al. (2007)
HgBr + Br → $HgBr_2$	6.95×10^{-11}	cm^3 $molec.^{-1}$ sec^{-1}	See note (a)
HgBr + BrO → Hg(OBr)Br	6.95×10^{-11}	cm^3 $molec.^{-1}$ sec^{-1}	(= $k_{HgBr + Br}$)
	Scenario 4		
Hg + Br + M → HgBr + M	2.79×10^{-32} exp(112/T) [M]	cm^3 $molec.^{-1}$ sec^{-1}	Shepler et al. (2007)
HgBr + M → Hg + Br + M	2.94×10^{-9} exp(-7670/T)	cm^3 $molec.^{-1}$ sec^{-1}	Shepler et al. (2007)
HgBr + Br → $HgBr_2$	2.98×10^{-11}	cm^3 $molec.^{-1}$ sec^{-1}	Balabanov et al. (2005)
HgBr + BrO → Hg(OBr)Br	2.98×10^{-11}	cm^3 $molec.^{-1}$ sec^{-1}	(= $k_{HgBr + Br}$)

Note: (a) The sum of the rate constants for Br-addition (R3a) and Br-exchange (R3b) channels as calculated by Balabanov et al. (2005).

Table 2: List of sub-category scenarios assumed for the gas-phase reaction HgBr + BrO and the rate of in-snow Hg(II) photo-reduction.

Scenario sub-category	A	B	C
Gas-phase reaction HgBr + BrO	On	On	Off
In-snow photo-reduction of Hg(II)	Slow	Fast	Slow

2.2 Results and discussion

Changes in mercury chemistry are irrelevant to the chemistry of bromine and ozone in our model runs (and perhaps so also in the real atmosphere). On the other hand, changes in the LLL diffusivity exert noticeable influences; delays in the simulated timescale of ODEs are often not negligible but generally minor, i.e., less than 1 day (see Fig. 3a-c, which is equivalent to Fig. 6a-c in Toyota et al., 2013a). Hence this part of update will not fundamentally modify our discussion in Toyota et al. (2013a) except for minor changes in stated numbers. Discussion in Toyota et al. (2013b) on the behavior of deposited Hg in the snowpack needs somewhat major changes as a result of reduced diffusivity in the LLL. As indicated from Fig. 4a-c (equivalent to Fig. 3a-c in Toyota et al., 2013b), most discussion in regard to mercury speciation in the atmosphere will remain the same except for the role of gas-phase reactions involving HgBr.

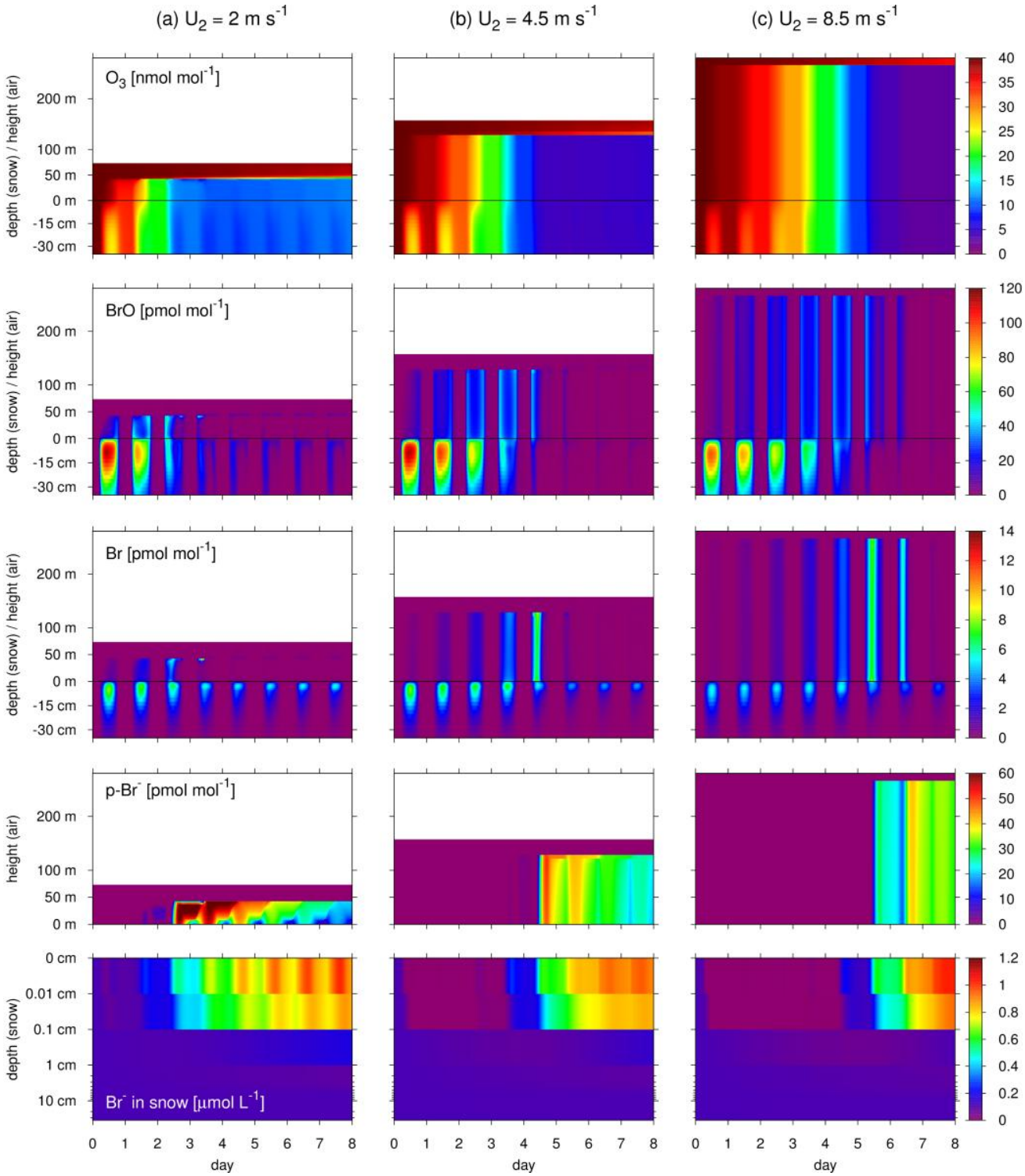

Figure 3: Time-height cross sections for the mixing ratios of O_3 (top row), BrO (second row), Br-atom (third row), and aerosol bromide (p-Br^-, fourth row), and for the bulk concentrations of bromide in snowpack grains (bottom row) from model runs with U_2 =2 m/s **(a)**, 4.5 m/s **(b)**, and 8.5 m/s **(c)**. For all the model runs, the scenario 2A is adopted for mercury chemistry (although not critical to the simulated behavior of ozone and bromine).

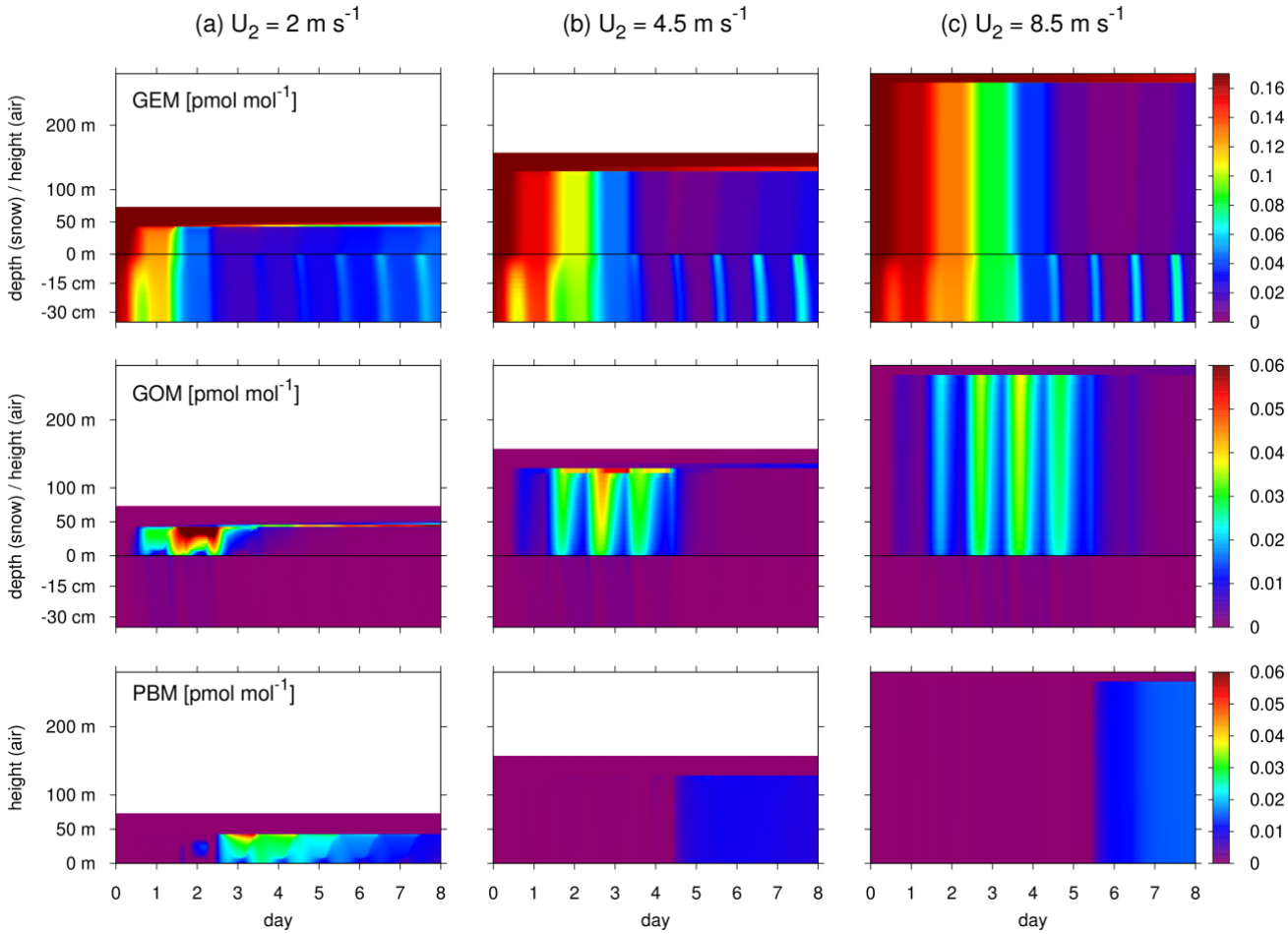

Figure 4: Time-height cross sections for the mixing ratios of GEM (top row), GOM (middle row), and PBM (bottom row) from model runs with U_2 = 2 m/s **(a)**, 4.5 m/s **(b)**, and 8.5 m/s **(c)**. For all the model runs, the scenario 2A is adopted for mercury chemistry.

Major impacts of changing the model scenarios for mercury chemistry are seen in the rate of GEM decrease and GOM increase during the progress of ODEs/AMDEs. In some scenarios, the concentrations of total gaseous mercury (TGM, = GEM + GOM) and ozone (at the height of 1.5m in the air) exhibit a compact linear relationship as often observed in the springtime coastal air in both hemispheres (e.g., Schroeder et al., 1998; Ebinghaus et al., 2002), whereas in others the relationship between TGM and ozone becomes apparently non-linear by accelerated/decelerated GEM-to-GOM conversion or more scattered by faster in-snow photo-reduction of Hg(II) and subsequent emissions of GEM back to the ambient air (see Fig. 5a-l, equivalent to Fig. 10a-c in Toyota et al., 2013b).

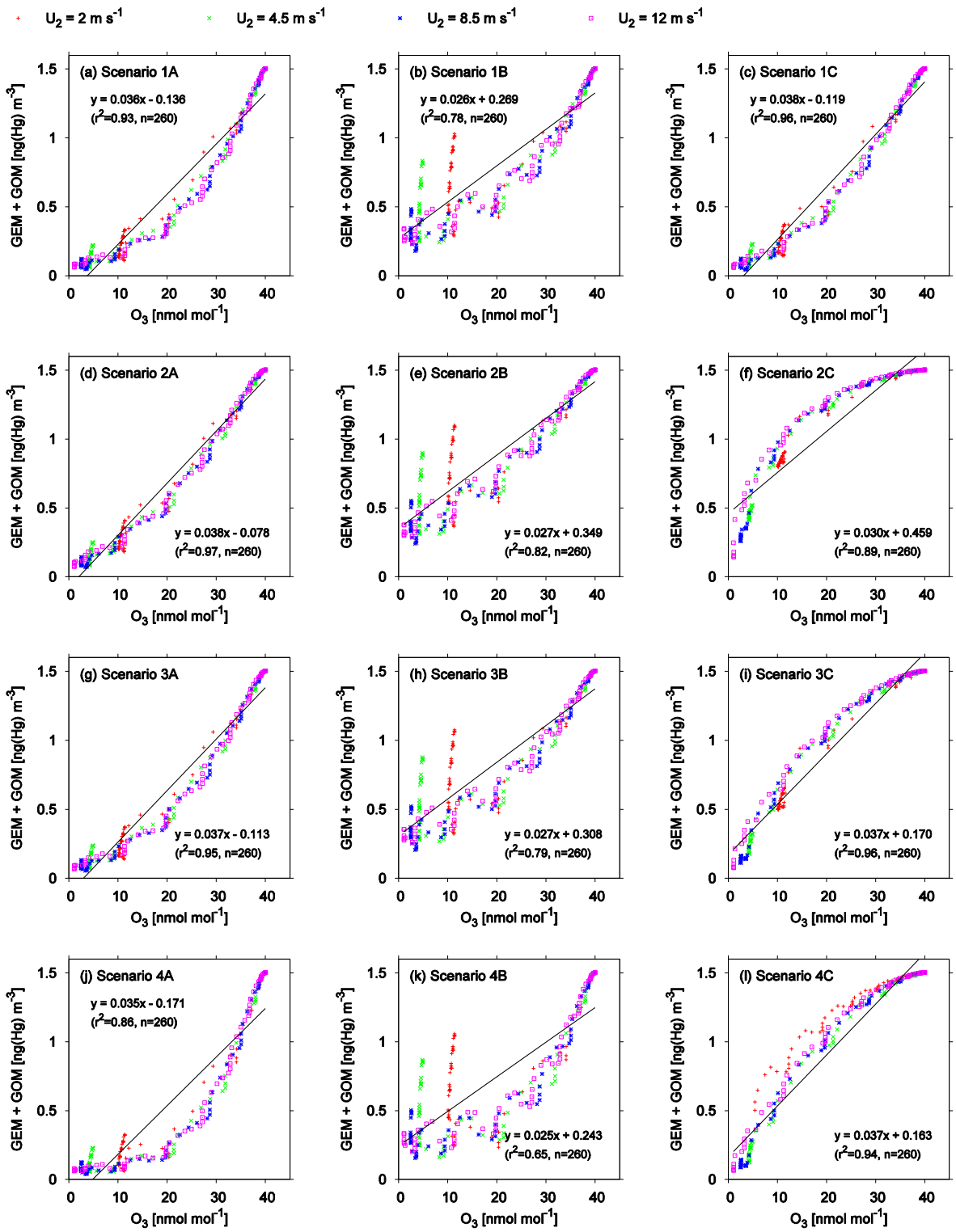

Figure 5: Scatter plots of 3-hourly model output to show correlations between the concentrations of total gaseous mercury (GEM + GOM) and the mixing ratios of ozone at the height of 1.5m in the ambient air as simulated in model runs at U_2 =2 m/s, 4.5 m/s, 8.5 m/s, and 12 m/s for each scenario of mercury chemistry (see Tables 1-2).

If we adopt the high rate constant for HgBr + Br → $HgBr_2$ (R3a) from Goodsite et al. (2004), viz. Scenarios 1A-C, the most compact linear relationship between TGM and ozone is obtained in Scenario 1C where we switch off the reaction HgBr + BrO for the formation of GOM. On the contrary, if we adopt the low rate constant for R3a from Balabanov et al. (2005), viz. Scenarios 2A-C, the depletion of TGM from the ambient air appears to be simulated rather too slowly without the reaction HgBr + BrO; Scenario 2A, in which this reaction is turned on, appears more realistic as it gives a more compact linear relationship. If we raise the rate constant for R3a by assuming that the occurrence of Br-exchange channel (R3b) as theoretically predicted in the low-pressure limit by Balabanov et al. (2005) actually gives rises to Br-addition (R3a) in the high-pressure limit at 1 atm, viz. Scenarios 3A-C, relationships between TGM and ozone are moderately "non-linear" both with and without the reaction HgBr + BrO where the shape of ozone-TGM correlation curves is hollow for Scenario 3A and bulge for Scenario 3C. In this case, accelerating the in-snow photoreaction of Hg(II) modify the hollow shape of the ozone-TGM correction curve with the reaction HgBr + BrO towards somewhat more linear trends, albeit with more scatters. Finally, if we turn back to the low rate constant for R3a from Balabanov et al. (2005) but now raise the rate constant for Hg + Br → HgBr (R1) based on Shepler et al. (2007), viz. Scenarios 4A-C, TGM depletion from the ambient air appears to proceed too rapidly when the reaction HgBr + BrO is turned on (Scenario 4A). In this case, the hollow shape of general trends in the ozone-TGM correlation does not vanish by raising the rates of in-snow Hg(II) photo-reduction (Scenario 4B). If we switch off the reaction HgBr + BrO instead, the general shape of ozone-TGM correlation turns from hollow to bulge, whilst this scenario (4C) gives the ozone-TGM correlation closer to a linear relationship than Scenario 4A.

3 Summary

Since the present model runs do not account for variability in meteorological conditions, especially temperature, which is most likely critical to changes in the rate constants for key reactions such as HgBr → Hg + Br (R2), we should not be able to conclude which pair of rate constants for mercury chemistry best represent the reality. It is also obvious that we have to handle too many free parameters in this exercise to achieve our goal of pinning down the kinetics and mechanism of mercury redox chemistry in the polar environment. Nonetheless, this sensitivity study indicates that uncertainty in the following kinetic parameters needs to be reduced to improve our modeling capability of mercury deposition from the air during AMDEs:

1. The rate constant in the high-pressure limit at ~1 atm for the reaction HgBr + Br for different product channels (R3a-c) to narrow down a factor of 8 discrepancy between Goodsite et al. (2004) and Balabanov et al. (2005);
2. The feasibility of the reaction HgBr + BrO to form thermally stable product(s) and, if it does, its rate constant, not studied to date experimentally except for theoretical calculations of bond energies that indicate the viability of the reaction in the atmosphere (Dibble et al., 2012);

3. The rate constant for the reaction of HgBr → Hg + Br (R2) and its temperature dependence to narrow down a factor of 4-5 discrepancy between Shepler et al. (2007) and Goodsite et al. (2012); and
4. The rate constant for Hg + Br → HgBr (R1) and its temperature dependence to narrow down a factor of 2 discrepancy between Donohue et al. (2006), Shepler et al. (2007) and Goodsite et al. (2012).

Referecences

Ariya, P. A., Khalizov, A., and Gidas, A.: Reactions of gaseous mercury with atomic and molecular halogens: kinetics, product studies, and atmospheric implications, J. Phys. Chem. A, 106, 7310–7320, 2002.

Balabanov, N. B., Shepler, B. C., and Peterson, K. A.: Accurate global potential energy surface and reaction dynamics for the ground state of $HgBr_2$, J. Phys. Chem. A, 109, 8765–8773, 2005.

Carignano, M. A., Shepson, P. B., and Szleifer, I.: Ions at the ice/vapor interface, Chem. Phys. Lett., 436, 99-103, 2007.

Dibble, T. S., Zelie, M. J., and Mao, H.: Thermodynamics of reactions of ClHg and BrHg radicals with atmospherically abundant free radicals, Atmos. Chem. Phys., 12, 10271-10279, doi:10.5194/acp-12-10271-2012, 2012.

Dibble, T. S., Zelie, M. J., and Mao, H.: Corrigendum to "Thermodynamics of reactions of ClHg and BrHg radicals with atmospherically abundant free radicals" published in Atmos. Chem. Phys. 12, 10271–10279, 2012, Atmos. Chem. Phys., 13, 9211-9212, doi:10.5194/acp-13-9211-2013, 2013.

Donohoue, D. L., Bauer, D., Cossairt, B., and Hynes, A. J.: Temperature and pressure dependent rate coefficients for the reaction of Hg with Br and the reaction of Br with Br: a pulsed laser photolysis-pulsed laser induced fluorescence study, J. Phys. Chem. A, 110, 6623–6632, 2006.

Ebinghaus, R., Kock, H. H., Temme, C., Einax, J. W., Lowe, A. G., Richter, A., Burrows, J. P., and Schroeder, W. H.: Antarctic springtime depletion of atmospheric mercury, Environ. Sci. Technol., 36, 1238–1244, 2002.

Goodsite, M. E., Plane, J. M. C., and Skov, H.: A theoretical study of the oxidation of Hg0 to HgBr2 in the troposphere, Environ. Sci. Technol., 38, 1772–1776, 2004.

Goodsite, M. E., Plane, J. M. C., and Skov, H.: Correction to A Theoretical Study of the Oxidation of Hg0 to HgBr2 in the Troposphere, Environ. Sci. Tech., 46, 5262–5262, doi:10.1021/es301201c, 2012.

Johnson, K. P., Blum, J. D., Keeler, G. J., and Douglas, T. A.: Investigation of the deposition and emission of mercury in arctic snow during an atmospheric mercury depletion event, J. Geophys. Res., 113, D17 304, doi:10.1029/2008JD009893, 2008.

Khalizov, A. F., Viswanathan, B., Larregaray, P., and Ariya, P. A.: A theoretical study on the reactions of Hg with halogens: atmospheric implications, J. Phys. Chem. A, 107, 6360–6365, 2003.

Kirk, J. L., St. Louis, V. L., and Sharp, M. J.: Rapid reduction and reemission of mercury deposited into snowpacks during atmospheric mercury depletion events at Churchill, Manitoba, Canada, Environ. Sci. Tech., 40, 7590–7596, 2006.

Schroeder, W. H., Anlauf, K. G., Barrie, L. A., Lu, J. Y., Steffen, A., Schneeberger, D. R., and Berg, T.: Arctic springtime depletion of mercury, Nature, 394, 331–332, 1998.

Shepler, B. C., Balabanov, N. B., and Peterson, K. A.: Hg + Br → HgBr recombination and collision-induced dissociation dynamics, J. Chem. Phys., 127, 164 304, doi:10.1063/1.2777142, 2007.

Toyota, K., McConnell, J. C., Staebler, R. M., and Dastoor, A. P.: Air-snowpack exchange of bromine, ozone and mercury in the springtime Arctic simulated by the 1-D model PHANTAS – Part 1: In-snow bromine

activation and its impact on ozone, Atmos. Chem. Phys. Discuss., 13, 20341-20418, doi:10.5194/acpd-13-20341-2013, 2013a.

Toyota, K., Dastoor, A. P., and Ryzhkov, A.: Air-snowpack exchange of bromine, ozone and mercury in the springtime Arctic simulated by the 1-D model PHANTAS – Part 2: Mercury and its speciation, Atmos. Chem. Phys. Discuss., 13, 22151-22220, doi:10.5194/acpd-13-22151-2013, 2013b.